Available online at www.sciencedirect.com
SCIENCE DIRECT
Polymer 47 (2006) 2172–2178
polymer
www.elsevier.com/locate/polymer

Metastability of polymer crystallites formed at low temperature studied by ultra fast calorimetry: Polyamide 6 confined in sub-micrometer droplets vs. bulk PA6

R.T. Tol [a,*], A.A. Minakov [b], S.A. Adamovsky [b], V.B.F. Mathot [a], C. Schick [b]

[a] *SciTe, Ridder Vosstraat 6, 6162 AX, Geleen, The Netherlands*
[b] *Inst. of Physics, University of Rostock, Universitätsplatz 3, 18051 Rostock, Germany*

Received 25 August 2005; received in revised form 3 January 2006; accepted 12 January 2006
Available online 3 February 2006

Abstract

It is shown that the application of a chip calorimeter, allowing very fast cooling and heating rates up to 10,000 K/s, can be successfully applied to study reorganization phenomena in crystallizable polymers. In this research both bulk Polyamide 6 (PA6) as well as an immiscible (polystyrene/styrene-maleic anhydride copolymer)/Polyamide 6 blend with dispersed Polyamide 6 droplets of sub-micrometer size have been studied. The blends with sub-micrometer PA6 droplets have been shown to crystallize at low temperature via a homogeneous nucleation mechanism, due to a lack of heterogeneities in the small droplets.

Upon fast cooling with more than 500 K/s crystallization of PA6 could be totally prevented. No cold crystallization takes place upon subsequent heating with 500 K/s. Upon fast heating of 2000 K/s after isothermal crystallization, the 'real', initial melting of the crystallites formed at very low temperature could be obtained, which was not possible with standard DSC apparatus or HPer DSC. However, even heating with 5000 K/s was not fast enough to completely avoid reorganization. Annealing experiments in the melt-range clearly show the fast reorganization of PA6 crystallites, resulting in improved stability within a timescale in the order of 0.01–0.1 s. Most probably reorganization takes place mainly in the crystalline state, and only to a lesser extent via a melting–recrystallization–remelting process. The reorganization process is not hindered by the confined dimensions of the Polyamide 6 droplets, because both bulk PA6 as well as the confined (PS/SMA2)/PA6 blend give rise to identical reorganization phenomena.

Keywords: Fast calorimetry; Reorganization; Polyamide 6

1. Introduction

Due to their long chain nature, crystallizable polymers are usually not in equilibrium. The crystal structure with the lowest free energy, build up by many fully extended chains, is seldom realized and the polymer chains are usually crystallized into a metastable state. Therefore, they usually show significant reorganization of their crystalline structure when held at temperatures between T_c and T_m [1–5]. This is especially apparent for small and imperfect crystals formed at high supercoolings, i.e. quenched samples, which are frequently obtained in industrial processing. However, significant supercoolings for crystallization can also be obtained when polymer chain segments are confined in space of small dimensions, even without quenching. In case dimensions are very small, active heterogeneities can become restricted to a relatively small fraction of the material, resulting in supercoolings as large as 150 °C below T_m leading to homogeneous nucleation kinetics [6–11]. Such crystallization phenomena have been observed for polymer chains in a wide variety of systems of small dimensions: block copolymers [6,7,19,12–17], dewetted films [8,9], polymer dispersions [18–22], and immiscible polymer blends [23–26] in which the crystallizable component forms domains of micro—or even nanosized dimensions. Reorganization phenomena can be expected to become very pronounced in these materials. Indeed, evidence for strong reorganization during the subsequent heating step has been reported [11,16,27] for crystals formed at high supercoolings. Using standard DSC it

* Corresponding author. Present address: Materials & Research, Research & Development, Toyota Motor Europe, Hoge Wei 33, B-1930 Zaventem, Belgium. Tel.: +32 2 712 3292; fax: +32 2 712 3326.
E-mail addresses: rob.tol@toyota-europe.com (R.T. Tol), vincent.mathot@scite.nl (V.B.F. Mathot), christoph.schick@uni-rostock.de (C. Schick).
URL: http://www.scite.nl.

0032-3861/$ - see front matter © 2006 Elsevier Ltd. All rights reserved.
doi:10.1016/j.polymer.2006.01.052

was not possible to observe the 'real' melting point distribution connected to the low temperature of crystallization of the crystals because of the fast reorganization process [11].

To regain the relation between the structure obtained in cooling and the melting behavior there is clearly a need for higher heating rates. It was shown by Pijpers et al. [28] that via a number of modifications of a standard power-compensated DSC setup, named High Performance DSC (HPer DSC), controlled and constant heating rates up to 500 K/min can be realized. However, to study reorganization processes, usually much faster heating rates are necessary, as was shown by Schick et al. recently. [29]. They showed that heating rates of more than 2000 K/s were necessary to prevent reorganization of PET crystals formed at low temperature. These measurements became possible due to developments in thin-film (chip) calorimetry, allowing very high heating rates up to 100,000 K/s, as shown by Allen et al. [30,31]. Schick et al. [29,32–35] developed a chip calorimeter operating under ambient conditions, allowing both fast, controlled heating and fast cooling up to 10,000 K/s. Recently, this chip calorimeter was used to study the origin of the multiple melting behavior of iPS [36].

In this paper we aim to prevent cold crystallization and reorganization during heating of Polyamide 6 (PA6) crystals formed at low temperature, by applying very fast heating using a thin-film chip calorimeter. Two samples will be compared. The first one is an immiscible blend, consisting of sub-micrometer PA6 droplets dispersed in a PS/SMA2 matrix. In a previous series of papers, Tol et al. [11,25] have shown that the crystallization of the PA6 droplets was delayed down to 85 °C, more than 100 °C below the usual bulk crystallization temperature. The second one is pure, bulk PA6. By using the chip calorimeter we intend to realize 'real' melting of the highly supercooled crystals and link it to the (confined) crystallization history.

2. Experimental

2.1. Materials and blend preparation

Polyamide 6 (PA6) with a molar mass of 24,000 g/mol was provided by DSM, Geleen, The Netherlands (PA Akulon K123). PS (PS Styron E680) was supplied by DOW Benelux, Terneuzen, The Netherlands and has a molar mass of 190,000 g/mol. A styrene-maleic anhydride copolymer (SMA2) (SEA 0579) with molar mass 145,000 g/mol was provided by Bayer, Dormagen, Germany and is miscible with PS over the full composition range [37,38]. The number after SMA denotes the mass percentage maleic anhydride in SMA. A blend with sub-micrometer PA6 droplets having diameters of about 0.15 μm was obtained by melt-mixing 25 m% PA6 and 75 m% of a (82/18 m/m) miscible mixture of polystyrene (PS) and styrene-maleic Anhydride copolymer (SMA2). Further details on the blend preparation can be found in a previous paper [39]. The SMA2 copolymer acts as a reactive compatibilizer and reduces the high interfacial tension between the two immiscible polymers PA6 and PS, giving rise to a stable blend morphology with fine and uniform PA6 droplets dispersed in the PS/SMA2 matrix. Because PA6 crystallization is strongly sensitive towards melt-extrusion (the PA6 crystallization temperature generally rises about 15 °C after extrusion [40]), pure PA6 was extruded under identical conditions as the blends prior to thermal analysis.

2.2. HPer DSC measurements

Fast DSC experiments were performed using a Perkin–Elmer Pyris Diamond DSC and nitrogen as purge gas. The instrument was calibrated by Indium and Zinc for temperature and by Sapphire for heat flow rate. The sample was wrapped in Aluminum foil of a few milligrams to minimize thermal lag [28].

2.3. Chip calorimeter measurements

2.3.1. Chip calorimeter set-up

Calorimetric experiments were performed with a thin-film chip calorimeter, developed by Schick et al. [29,32–35], based on the thermal conductivity gauge TCG-3880 from Xensor Integration, The Netherlands [41]. The thermal conductivity gauge TCG-3880 consists of a 0.5 μm Si_3N_x membrane with a thin-film thermopile and a resistive thin film-heater placed at the center of the membrane. A schematic overview of the set-up is given in Fig. 1. To allow fast cooling rates, the cell was operated under non-adiabatic conditions, in ambient gas. Because the heat capacities and thermal resistances of the

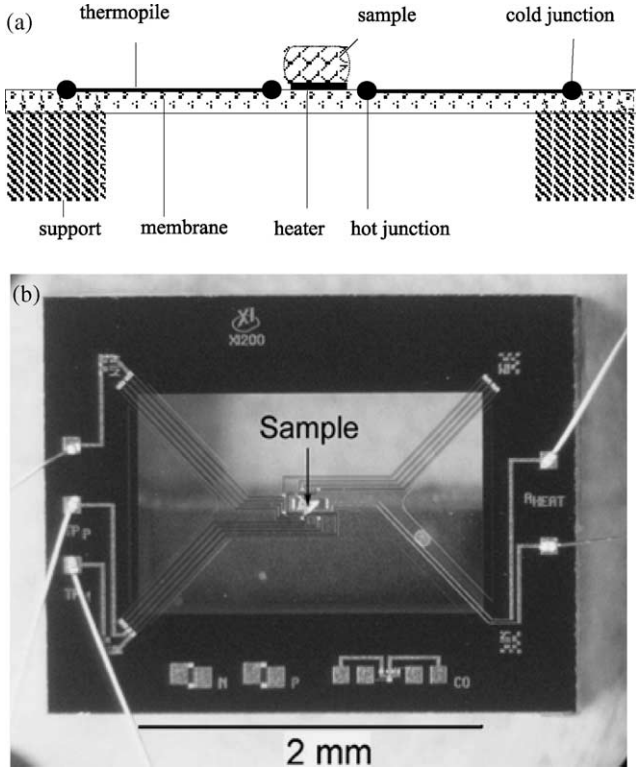

Fig. 1. Schematic overview (a) and micro-photograph (b) of the frame and membrane of the chip-calorimeter.

thin film-heater and of the thermopile are negligibly small, the addenda heat capacity is the effective heat capacity of the heated part of the membrane. As such, the following heat balance equation can be used, provided that the thermal thickness of the sample is small enough and the heat transfer from the sample to the thermostat can be described by Newton's law:

$$(C + C_0)\frac{dT}{dt} = \Phi_0(t) - \xi(T(t) - T_0) \quad (1)$$

C_0 is the effective heat capacity of the central part of the membrane, C the heat capacity of the sample. T is the temperature of the heated region of the membrane. $\Phi_0(t)$ is the heat flow rate, provided by the resistive thin film-heater. ξ is the heat-exchange coefficient (in W/K), which depends on the specific ambient gas applied. T_0 is the temperature of the environment, which is close to the temperature of the sample holder (see Fig. 1A). This temperature is measured using an additional copper/constantan thermocouple. However, the measured temperature does not represent the temperature of the heater/sample interface because the thermopile measures the temperature at the membrane around the heater. Thus, the measured temperature needs to be calibrated as described in [32].

To determine whether the sample thickness was small enough to avoid large temperature gradients in the sample, the following equation for calculating the temperature gradient across a plate-like sample of thickness d was used

$$\Delta T = (dT/dt)(d^2\rho c/\lambda) \quad (2)$$

where ρ, c and λ are the density, the specific heat capacity and the thermal conductivity of the sample, respectively. For polystyrene (PS) ΔT equals 3 K at $d = 10$ μm and 12 K for 20 μm for a heating rate of 2000 K/s, and a thermal conductivity of 0.13 W/(m K) [42]. The heat flow rate, $\Phi_0(t)$ is provided by the resistive film-heater, which is determined by the electrical current in the heater $I_h(T)$ and its resistance $R_h(T)$, which was calibrated in advance [32]. The electric current in the heater was monitored during its scanning simultaneously with the temperature difference $T(t) - T_0$ measured by the thermopile. The temperature dependence of the thermopile sensitivity was calibrated as described in [32]. The heat, which is supplied to the membrane/sample interface, propagates through the membrane, sample and ambient gas. Because the membrane is very thin the heat transfer through the ambient gas is dominant. Furthermore, the heat transfer in the radial (horizontal in Fig. 1A) direction is small compared to the heat transfer in perpendicular (vertical in Fig. 1A) direction [32].

Thus, there are three unknown parameters in Eq. (1): ξ, C_0 and C. The parameter $C_0(T)$ was determined in advance for the empty cell. The parameters ξ and C can be determined from heating and cooling scans as described in [32]. As the gas thermal conductivity depends on temperature, the heat exchange coefficient ξ is also a function of temperature. The temperature dependence of the heat exchange coefficient can be approximated by a smooth monotonous polynomial function [32] and was determined according to the procedure described in [29]. To determine the specific heat capacity the sample mass has to be known. The sample mass was not measured independently but was determined from the measured heat capacity and the known specific heat capacity in the molten state [43]. Here, the heat capacity of the SMA2 copolymer, which is not listed in the ATHAS databank, was taken equal to the heat capacity of pure PS, assuming that the low amount of maleic-anhydride groups will not significantly affect the heat capacity signal.

2.3.2. Sample preparation and measuring conditions

The cell was operated in nitrogen gas to avoid oxidative degradation of PA6 and the holder temperature was −10 °C. The sample was moved to the top of the heater of the calorimetric sensor by a soft copper wire, to avoid damaging of the sensor membrane. As a temperature gradient exists in the radial direction along the membrane, the sample has to be placed just on the heater in order to avoid a temperature gradient on the periphery of the sample outside the heated area. The sample was fixed at the position just on the top of the heater by switching on an electrical current through the heater, which melted the sample. All samples were heated to about 250 °C for 0.1 s prior to the cooling run. It turned out that this was sufficient to avoid melt-memory effects (self-seeding).

For the isothermal crystallization experiments the sample was cooled fast at 2000 K/s from the melt to the particular crystallization temperature. After crystallization, the sample was cooled down fast (2000 K/s) to −10 °C prior to heating. The reorganization experiments were performed as follows: after isothermal crystallization at 85 °C and fast cooling to −10 °C, the sample was heated fast (also 2000 K/s) to a temperature T_{ann}, in the melting region, where the crystals were allowed to reorganize at this temperature during a time $t_{ann.}$. Then the sample was cooled fast with 2000 K/s to −10 °C to avoid further crystallization during the cooling. Finally, the sample was heated fast again. The temperature program is given in Fig. 2.

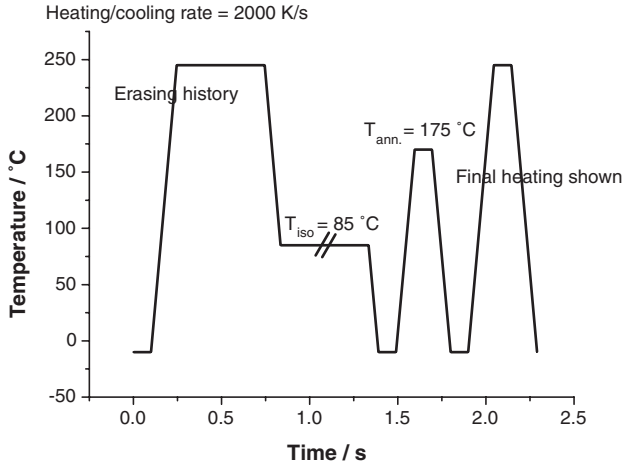

Fig. 2. Temperature program for annealing experiments.

3. Results and discussion

3.1. Fast cooling and subsequent fast heating

Fig. 3 shows the heating curves (500 K/s) after cooling with 500 K/s for bulk PA6 and the (PS/SMA2)/PA6 (62/13)/25 blend with sub-micrometer sized PA6 droplets. As can be seen both the (PS/SMA2)/PA6 blend and bulk PA6 can be quenched into the amorphous state by using a cooling rate of 500 K/s. Upon subsequent heating, (cold) crystallization can be avoided completely and no melting trace is observed. As such, this opens up the possibility to study crystallization kinetics in a way not possible before.

3.2. Isothermal crystallization and subsequent fast heating

Fig. 4 shows the cooling and melting of the (PS/SMA2)/PA6 blend with PA6 droplets of about 0.15 μm dispersed in the PS/SMA2 matrix measured with a PerkinElmer Diamond DSC. We have chosen to use 1 (one and the same) C_p scale for both cooling and heating (not the sometimes observed double positive C_p-axis (upwards for heating and downwards for cooling). The crystallization temperature in these droplets is strongly reduced. In two previous papers, it was shown that this was caused by crystallization of PA6 chains confined in droplets of small dimensions [11,25]. Due to the small dimensions, the number of heterogeneous nuclei is restricted to a limited portion of the droplets; the remaining heterogeneity-free droplets force the PA6 chains to crystallize via homogeneous nucleation, for which a much higher supercooling is needed. Although most of the material crystallized at about 85 °C, a melting peak is seen around 220 °C, after applying a standard heating rate of about 10 K/min. The mismatch between the areas under the crystallization and melting peaks clearly confirms that the crystals formed show strong reorganization during the heating run, with an exothermic contribution that is smeared out over the full temperature range between T_g PA6 (~50 °C) and T_m. It is, however, clear that also these high performance

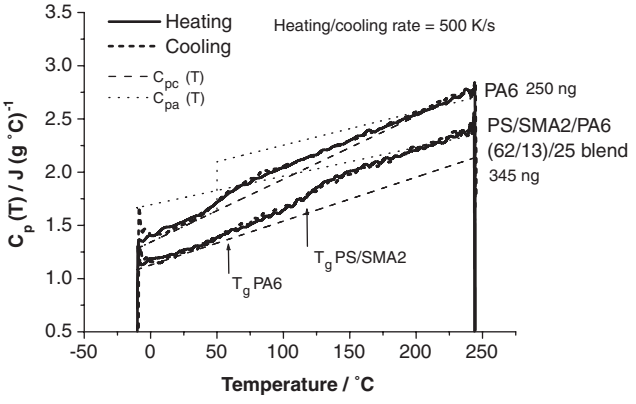

Fig. 3. Specific heat capacities in heating and cooling of approx. 245 ng PA6, approx. 345 ng (PS/SMA2)/PA6 (62/13)/25 blend. Heating and cooling rates: 500 K/s. $C_{pc}(T)$: specific heat capacity of crystalline phase from ATHAS databank, $C_{pa}(T)$: specific heat capacity of amorphous phase from ATHAS databank.

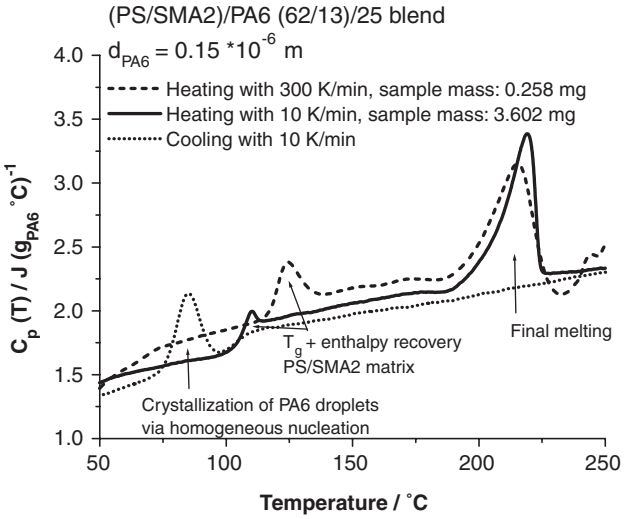

Fig. 4. Melting of (PS/SMA2)/PA6 (62/13)/25 blend after 10 K/min cooling to −10 °C at different heating rates measured with a Perkin Elmer Diamond DSC.

DSC measurements, here with a constant scanning rate of 300 K/min, fail to detect the 'real' melting behavior of these low temperature crystallized PA6 crystals, as the shape and position of the melting peak are not significantly affected by the applied heating rate. As can be concluded from the differences between the curves, though the measurements have been evaluated as heat capacities, the results are not really quantitative.

Fig. 5 shows the melting behavior after crystallization at different temperatures for the (PS/SMA2)/PA6 blend and bulk PA6 measured using the chip calorimeter. The fast cooling rate of 2000 K/s with the chip calorimeter enables a direct comparison of the melting behavior after isothermal crystallization for the PA6 in the confined geometry and the PA6 bulk upon crystallization from the melt at low temperatures, because no crystallization occurs upon approaching T_{iso} for bulk PA6 (see Fig. 3). There is a remarkable difference in melting behavior of both samples as a function of the crystallization temperature, reflecting the completely different nucleation mechanism of PA6 in the confined geometry compared to bulk

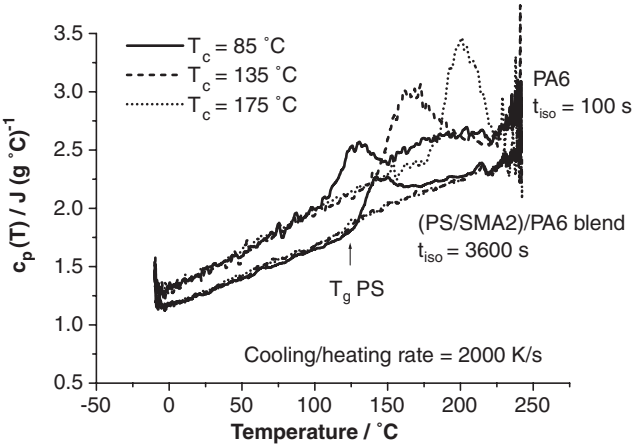

Fig. 5. Specific heat capacities in heating of PA6 and (PS/SMA2)/PA6 (62/13)/25 blend crystallized at different temperatures.

PA6; the (PS/SMA2)/PA6 blend does not crystallize at higher crystallization temperatures, not even at very long crystallization times, but is restricted to the temperature interval below about 100 °C. This is not the case for bulk PA6, where a single, broad melting peak is observed even at the relatively high crystallization temperature of 175 °C, connected to the 'real' melting of crystals formed around this temperature. Upon decreasing T_c, the melting temperature decreases accordingly and becomes broader. For both samples, however, a broad double melting peak is observed after crystallization at 85 °C for 1 h. The first melting peak can be related to the initial 'real' melting of the crystallites formed at 85 °C. The second, broad peak must, however, be interpreted to be connected to reorganization of the PA6 crystallites during heating. A heating rate of 2000 °C/s is thus still not enough to completely suppress reorganization of the PA6. Unfortunately, the initial melting of PA6 around 120 °C overlaps with an enthalpy recovery peak of the PS/SMA2 matrix phase in case of the (PS/SMA2)/PA6 blend. The enthalpy recovery peak is present because the sample was held just below the T_g of the (PS/SMA2) phase (which is at approximately 105 °C at a heating rate of 10 K/min) for 3600 s, by which it undergoes a relatively rapid physical aging (enthalpy relaxation) process at this temperature, as is clear from Fig. 6.

Fig. 7 shows the effect of different heating rates on the melting curves of the PA6 and the (PS/SMA2)/PA6 blend, crystallized at 85 °C. It is clearly seen that the first 'real' melting peak shifts to higher temperature and the second melting peak—caused by reorganization—to lower temperature with increasing heating rates. The shift to higher temperatures of the 'real' melting peak around 120 °C with increasing heating rate probably points to some superheating of the PA6 crystals. Similar shifts in melting points have been reported for other polymers when heated at such high rates [29,36]. The shift of the second, broad melting peak to lower temperatures clearly points to an increased hindering of reorganization during heating of the crystals formed at low temperature. The curves also suggest an increase in area of the lower melting peak at the expense of the second, higher melting peak with increasing heating rate, which confirms increasing

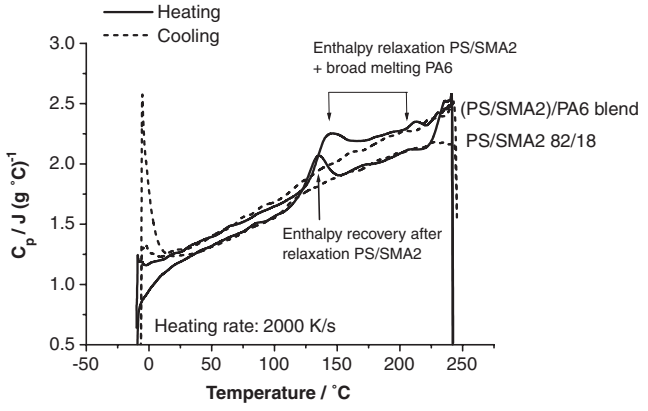

Fig. 6. Specific heat capacities for (PS/SMA2)/PA6 (62/13)/25 blend and PS/SMA2 82/18 mixture, measured at a heating rate of 2000 K/s after crystallization from the melt at 85 °C for 3600 s.

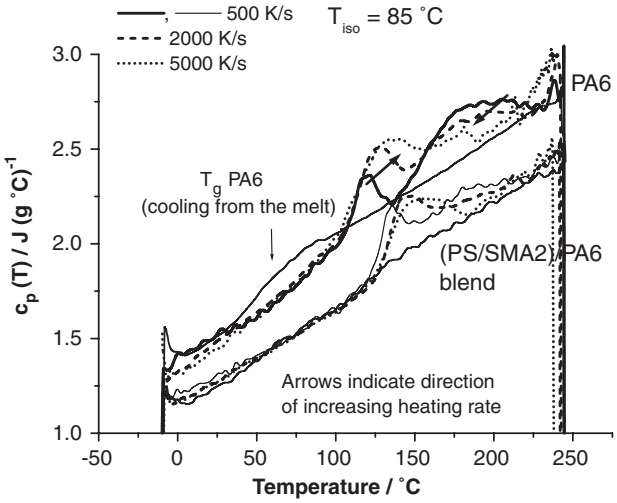

Fig. 7. Specific heat capacities of PA6 and (PS/SMA2)/PA6 (62/13)/25 blend, measured at different heating rates, after crystallization from the melt at 85 °C for 3600 s.

hindering of reorganization. The chip calorimeter experiments are thus clearly able to visualize the initial 'real' melting of the PA6 crystallites and to prevent reorganization phenomena upon heating to a large extent for both bulk and confined PA6.

3.3. Annealing in the melting region after isothermal crystallization

To determine the kinetics of the reorganization process, isothermal crystallization experiments were performed according to the temperature program described in Section 2.3.2. By heating up the sample at 2000 K/s to a temperature $T_{ann.}$ in the melting region (between 130 and 220 °C) after crystallization at 85 °C, the crystallites are allowed to reorganize at this temperature. Afterwards, the samples are cooled down at 2000 K/s to below T_g and the melting behavior after this annealing step is recorded at 2000 K/s. The very fast cooling rate will prevent any further primary crystallization, as was confirmed in Fig. 3.

In Fig. 8 the final melting run after a very short annealing time for both the (PS/SMA2)/PA6 (62/13)/25 blend as well as for bulk PA6 is shown. It can be seen that the initial melting peak shifts to higher temperatures, so obviously reorganization is happening on a very short time-scale. Because the blend is not able to crystallize at temperatures above 100 °C, see discussion with respect to Fig. 5 (while during cooling and following heating at 2000 K/s no primary crystallization can take place), the melting peaks have to be related to the isothermal crystallization at 85 °C and subsequent reorganization at 175 °C. The fact that this process is quite similar for both the confined (PS/SMA2)/PA6 blend and bulk PA6 points to the same cause: increasing stability of crystallites by fast reorganization at 175 °C.

In Fig. 9 the melting curves of bulk PA6 after applying different annealing temperatures are shown. Here, two effects can be distinguished. First of all, with increasing annealing temperatures, the low temperature melting peak shifts

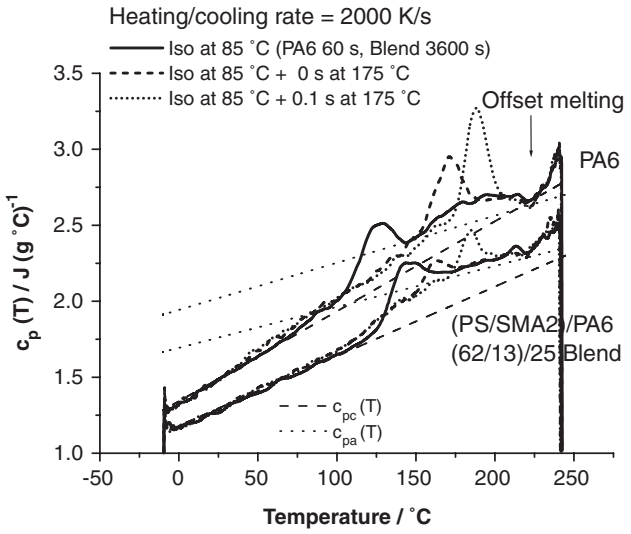

Fig. 8. Specific heat capacities, measured in heating at 2000 K/s after isothermal crystallization at 85 °C for 3600 s followed by isothermal reorganization at 175 °C, for bulk PA6 and (PS/SMA2)/PA6 (62/13)/25 blend. $C_{pc}(T)$: specific heat capacity of crystalline phase from ATHAS databank, $C_{pa}(T)$: specific heat capacity of amorphous phase from ATHAS databank.

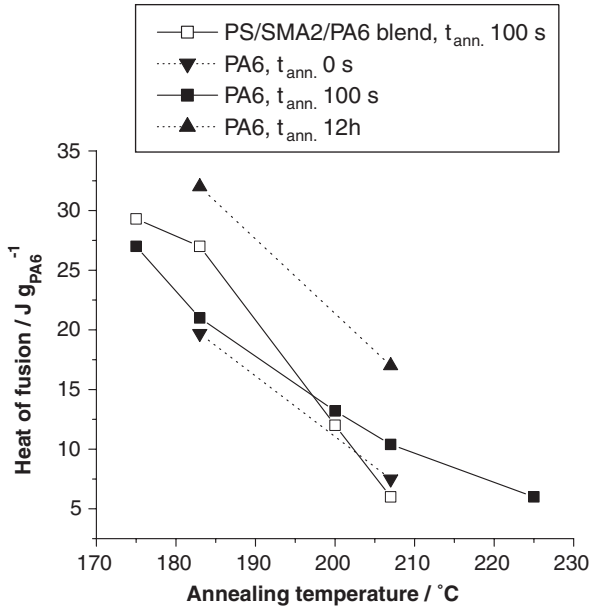

Fig. 10. Heat of fusion as a function of annealing temperature for (PS/SMA2)/PA6 (62/13)/25 blend and bulk PA6. For PA6: $t_{ann.}$: 0 s, 100 s and 12 h.

to higher temperatures, as expected. Interestingly, however, the heat of fusion strongly decreases with increasing annealing temperature. This effect can also be (indirectly) observed from the shape of the T_g transition of PA6, which can be found around 70 °C; the step in heat capacity at the T_g increases with increasing annealing times, pointing to a decrease in crystallinity.

Figs. 10 and 11 give the complete evolution of heat of fusion and melting temperature for various annealing temperatures. The heat of fusion of PA6 increases with increasing annealing time, as can be seen in Fig. 10, due to increasing perfection of the crystals with time. However, even for very long annealing times a similar decrease of heat of fusion with annealing temperature can be observed. As seen in Figs. 7 and 8, part of the crystals will quickly reorganize at the annealing temperature and increase their melting temperature. However, upon heating to the annealing temperature, part of the crystals will also melt, and will not crystallize during the annealing time nor during the subsequent cooling step (at 2000 K/s) as was shown in Fig. 3. Obviously, upon increasing the annealing temperature, the amount of material that is molten increases, which explains the continuous decrease in observed crystallinity with increasing annealing temperature. As such, the results indicate that the main reorganization event takes place in the crystallites formed at 85 °C, and within a quite short time scale. This time-scale can estimated to be shorter than ~100 °C/5000 K/s = 0.02 s, because scanning with 5000 K/s over a temperature range of 100 °C still gives some reorganization of PA6, as is seen from Fig. 7. Interestingly,

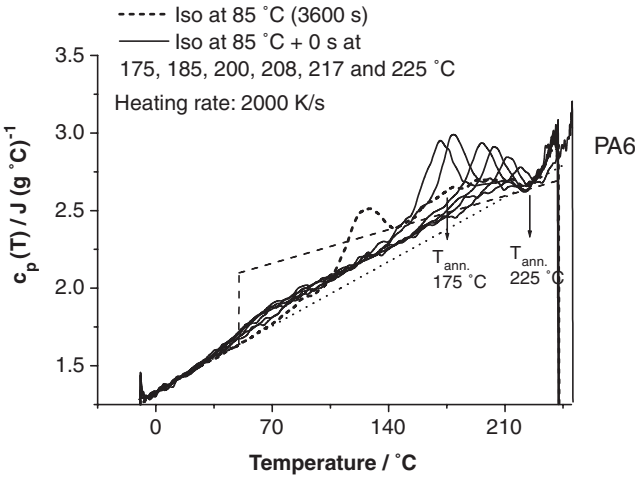

Fig. 9. Specific heat capacities, measured in heating at 2000 K/s after annealing at different temperatures between T_c and $T_{m,final}$, for bulk PA6.

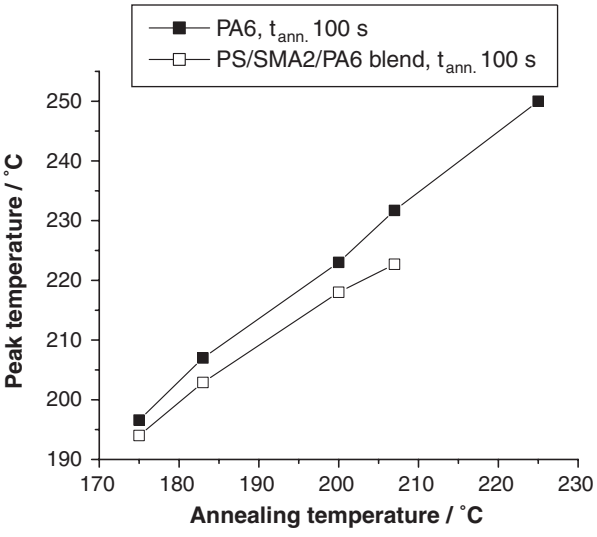

Fig. 11. Peak melting temperature as a function of annealing temperature for (PS/SMA2)/PA6 (62/13)/25 blend and bulk PA6. Annealing time was 100 s.

similar results were recently reported by Röttele et al. [27] for a confined copolymer system by combining DSC experiments with real-time AFM. A broad melting range was observed for nanometer confined PEO domains, which was related to the melting of individual crystals exhibiting a multitude of possible metastable states. These individual crystals then have the choice between complete melting or reorganization of the crystallites. The experiments presented in this paper clearly show that similar results can be obtained for a polymer in the bulk state. The results suggest that also in the case of bulk PA6 reorganization of existing crystallites takes place, though any melting—recrystallization–remelting process can still not be excluded.

4. Conclusions

It is shown that fast scanning chip calorimetry allows to amorphize bulk PA6 by fast cooling and to prevent any cold crystallization during subsequent fast heating. Using high cooling rates, it is therefore possible to isothermally crystallize bulk PA6 at any temperature above T_g. By applying a high heating rate, it is then possible to determine the 'real' melting of bulk PA6 crystals formed at any temperature chosen. By dispersing PA6 in droplets having sub-micrometer dimensions within a PS/SMA2 matrix, homogeneous nucleation of PA6 at very low temperatures has become feasible. In that way it is possible to isothermally crystallize PA6 dispersed in the matrix and bulk PA6 at low temperatures, e.g. at 85 °C. Heating at high enough rate prevents cold crystallization, by which only reorganization processes (and possibly also recrystallization) are possible. By fast heating with 5000 K/s the reorganization phenomena are largely suppressed, but cannot be completely avoided. The reorganization process of PA6 crystals in both the droplets within the blend as well as in bulk PA6 is very fast and seems to be mainly determined by the crystallization temperature and not so much by the confined geometry (150 nm diameter PA6 droplets) as both give rise to identical reorganization phenomena. Annealing of the structures that were isothermally crystallized at low temperature, at different temperatures in the melting region, indicate that reorganization mainly takes place in the crystallites formed during isothermal crystallization.

Acknowledgements

RT is indebted to European Community for COST P12 STSM grant hosted by SciTe. Financial support by the University of Rostock, SciTe and KULeuven is gratefully acknowledged.

References

[1] Al-Hussein M, Strobl G. Eur Phys J 2001;E6:305.
[2] Al-Hussein M, Strobl G. J Macromol Sci—Phys 2003;B42:677.
[3] Organ SJ, Hobbs JK, Miles MJ. Macromolecules 2004;37:4562.
[4] Sommer JU, Reiter G. Phase Transitions 2004;77:703.
[5] Mathot VBF, Scherrenberg RL, Pijpers TFJ. Polymer 1998;39(19):4541.
[6] Loo Y-L, Register RA, Ryan AJ. Phys Rev Lett 2000;84(18):4120.
[7] Reiter G, Castelein G, Sommer J-U, Röttele A, Thurn-Albrecht T. Phys Rev Lett 2001;87(22):226101.
[8] Massa MW, Carvalho JL, Dalnoki-Veress K. Eur J Phys E 2003;12(1): 111.
[9] Massa MW, Dalnoki-Veress K. Phys Rev Lett 2004;29:255509.
[10] Xu JT, Ryan AJ, Mai SM, Yuan JJ, Cheng SY. J Macromol Sci—Phys 2004;B43:685.
[11] Tol RT, Mathot VBF, Groeninckx G. Polymer 2005;46:2955.
[12] Lee W, Chen HL, Lin TL. J Polym Sci Part B: Polym Phys 2002; 40(6):519.
[13] Müller AJ, Balsamo V, Arnal ML, Jakob T, Schmalz H, Abetz V. Macromolecules 2002;35(8):3048.
[14] Vasilev C, Heinzelmann H, Reiter G. J Polym Sci Part B: Polym Phys 2004;42(7):1312.
[15] Müller AJ, Balsamo V, Arnal ML. Adv. Polym. Sci. Accepted for Publication.
[16] Xu JT, Zhao YQ, Liang GD, Fan ZQ. Polym J 2005;37(1):43.
[17] Cormia RL, Price FP, Turnbull D. J Chem Phys 1962;37(6):1333.
[18] Koutsky JA, Walton AG, Baer E. J Appl Phys 1967;38(4):1832.
[19] Montenegro R, Antonietti M, Mastai Y, Landfester K. J Phys Chem B 2003;107:5088.
[20] Montenegro R, Landfester K. Langmuir 2003;19(15):5996.
[21] Uriguen JI, Bremer L, Mathot VBF, Groeninckx G. Polymer 2004;45: 5961.
[22] Frensch H, Harnishfeger P, Jungnickel BJ. In: Utracki LA, Weiss RA, editors. ACS symposium series, vol. 395; 1989, p. 101
[23] Everaert V, Groeninckx G, Aerts L. Polymer 2000;41:1409.
[24] Tol RT, Mathot VBF, Groeninckx G. Polymer 2005;46(2):369.
[25] Tol RT, Mathot VBF, Groeninckx G. Polymer 2005;46(2):383.
[26] Tol RT, Mathot VBF, Reynaers H, Groeninckx G. In: Harrats C, Thomas S, Groeninckx G, editors. Phase morphology and interfaces in micro-and nanostructured immiscible polymer blend systems. Boca Raton/London/New York: CRC Taylor & Francis; 2006. p. 391–420.
[27] Röttele A, Thurn-Albrecht T, Sommer JU, Reiter G. Macromolecules 2003;36:1257.
[28] Pijpers TFJ, Mathot VBF, Goderis B, Scherrenberg RL, van der Vegte EW. Macromolecules 2002;35:3601.
[29] Minakov AA, Mordvintsev DA, Schick C. Polymer 2004;45:3755.
[30] Efremov MY, Olson EA, Zhang M, Allen LH. Macromolecules 2002; 35:1481.
[31] Efremov MY, Olson EA, Zhang M, Zhang Z, Allen LH. Phys Rev Lett 2003;91:857031–4.
[32] Adamovsky SA, Minakov AA, Schick C. Thermochim Acta 2003; 403(1):55.
[33] Adamovsky SA, Schick C. Thermochim Acta 2004;415:1.
[34] Minakov AA, Mordvintsev DA, Schick C. Faraday Discuss 2005;128: 261.
[35] Minakov AA, Adamovsky SA, Schick C. Thermochim Acta 2005; 432(2):177.
[36] Minakov AA, Mordvintsev DA,Tol R, Schick C., Thermochim Acta, in press.
[37] Fried JR, Hanna GA. Polym Eng Sci 1982;22:705.
[38] Wittler H, Leiser G, Drosher M. Makromol Chem Rapid Commun 1993; 14:401.
[39] Tol RT, Groeninckx G, Vinckier I, Moldenaers P, Mewis J. Polymer 2004;45:2587.
[40] Tol RT, Mathot VBF, Reynaers H, Goderis B, Groeninckx G. Polymer 2005;46:2966.
[41] van Herwaarden AW, Thermochim. Acta 2005;432:192 and http://www.xensor.nl/
[42] Material properties data base available at: http://www.goodfellow.com.
[43] ATHAS databank: http:web.utk.edu/~athas/databank.